Editors' Suggestion

# Multidimensional Atom Optics and Interferometry

B. Barrett,[1,2,*] P. Cheiney,[1,2] B. Battelier,[2] F. Napolitano,[1] and P. Bouyer[2]
[1]*iXblue, 34 rue de la Croix de Fer, 78105 Saint-Germain-en-Laye, France*
[2]*LP2N, Laboratoire Photonique, Numérique et Nanosciences, Université Bordeaux–IOGS–CNRS:UMR 5298, 1 rue François Mitterrand, 33400 Talence, France*

(Received 29 October 2018; published 1 February 2019)

We propose new multidimensional atom optics that can create coherent superpositions of atomic wave packets along three spatial directions. These tools can be used to generate light-pulse atom interferometers that are simultaneously sensitive to the three components of acceleration and rotation, and we discuss how to isolate these inertial components in a single experimental shot. We also present a new type of atomic gyroscope that is insensitive to parasitic accelerations and initial velocities. The ability to measure the full acceleration and rotation vectors with a compact, high-precision, low-bias inertial sensor could strongly impact the fields of inertial navigation, gravity gradiometry, and gyroscopy.

DOI: 10.1103/PhysRevLett.122.043604

Inertial sensors based on cold atoms and light-pulse interferometry [1–3] exhibit exquisite sensitivity that could potentially revolutionize a variety of fields including geophysics and geodesy [4,5], gravitational wave detection [6], tests of fundamental laws, and inertial navigation [7,8]. Their state-of-the-art sensitivity and ultralow measurement bias are particularly appropriate for long-term integration as in precision measurements [9,10] or space experiments [11]. They also offer great potential for autonomous inertial navigation systems [12–15], where the attitude and position of a moving body is determined by integrating the equations of motion.

The measurement principle of light-pulse atom interferometers (AIs) is linked to a retroreflected laser beam that is referenced to an atomic transition. This defines a phase ruler to which the free-falling atom's trajectory is compared [16], in analogy to classical falling-corner-cube gravimeters [17]. In general, the direction of the retroreflected beam defines the inertially sensitive axis of these quantum sensors. They can be sensitive to accelerations [18–22] and acceleration gradients [23–25] parallel to the effective optical wave vector $\boldsymbol{k}$, and to rotations perpendicular to the plane defined by $\boldsymbol{k} \times \boldsymbol{v}_0$ [26–32], where $\boldsymbol{v}_0$ is the initial velocity of the atomic source. So far, the challenge of realizing multiaxis inertial measurements has been addressed only in a sequential manner [33,34], where the direction of $\boldsymbol{k}$ was changed between measurement cycles. In this work, we propose new multidimensional AI geometries that are *simultaneously* sensitive to accelerations and rotations in three dimensions, and can discern their vector components within a single shot.

In what follows, we define a multidimensional AI as one where the light interaction exchanges momentum with the atomic sample along more than one spatial direction at a time. This momentum exchange is accompanied by an independent phase shift along each axis, which is imprinted on the corresponding diffracted wave packet [35]. This mechanism creates a unique type of atom-optical element that satisfies all the requirements of a multidimensional AI—enabling one to split, reflect, and recombine matter waves along two or more axes simultaneously.

We have developed a semiclassical model for 3D atom optics involving Raman transitions [36]. Figure 1 shows examples of 2D and 3D atom-optical beam splitters, where

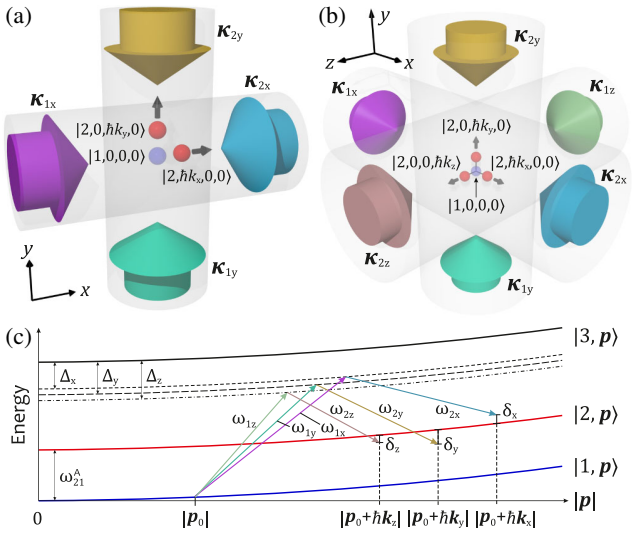


FIG. 1. (a), (b) Multidimensional atom-optical beam splitters realized with mutually orthogonal pairs of independent, counterpropagating Raman beams. (c) Energy-momentum diagram showing velocity-sensitive Raman transitions associated with each pair of beams shown in (a), (b). To avoid excitation of parasitic resonances, different detunings $\Delta_\mu$ are used for each beam pair. This leads to a small difference in the wave vectors $k_\mu$, which has been exaggerated for clarity.

 

mutually orthogonal pairs of counterpropagating Raman beams couple an atom with initial momentum $\boldsymbol{p}_0$ to two or three diffracted states moving perpendicular to one another. Along each axis $\mu = x, y, z$, two beams with wave vectors $\boldsymbol{\kappa}_{1\mu}$ and $\boldsymbol{\kappa}_{2\mu}$, and corresponding frequencies $\omega_{1\mu}$ and $\omega_{2\mu}$, excite two-photon Raman transitions [37] between two ground states $|1\rangle$ and $|2\rangle$ separated by frequency $\omega_{21}^{\mathrm{A}}$. During this process, a momentum $\hbar\boldsymbol{k}_\mu = \hbar(\boldsymbol{\kappa}_{1\mu} - \boldsymbol{\kappa}_{2\mu})$ is transferred to the atom, where $\hbar$ is the reduced Planck's constant and $\boldsymbol{k}_\mu \simeq 2\boldsymbol{\kappa}_{1\mu}$ is the effective Raman wave vector along axis $\mu$ [38,39]. The laser frequencies $\omega_{n\mu}$ are detuned by $\Delta_\mu$ from an intermediate excited state $|3, \boldsymbol{p}_0\rangle$ as shown in Fig. 1(c), such that $|\Delta_\mu|$ is large compared to the natural linewidth of the atomic transition and, for $\mu \neq \nu$, $|\Delta_\mu - \Delta_\nu|$ is much larger than the effective Rabi frequency. This second condition strongly inhibits scattering processes involving absorption along one axis and reemission along another. In the region of beam overlap, an atom initially in $|1, \boldsymbol{p}_0\rangle$ undergoes 3D diffraction—splitting the wave packet into a superposition of this undiffracted state and three orthogonal diffracted states: $|2, \boldsymbol{p}_0 + \hbar\boldsymbol{k}_\mu\rangle$. The dynamics of this coherent 3D diffraction process are described by Rabi oscillations in an effective 4-level system: $|\Psi\rangle = \mathcal{C}_0|1,0,0,0\rangle + \mathcal{C}_x|2,\hbar k_x,0,0\rangle + \mathcal{C}_y|2,0,\hbar k_y,0\rangle + \mathcal{C}_z|2,0,0,\hbar k_z\rangle$, where the states are labeled by their internal energy and the photon momentum transfer along each direction. This system exhibits Rabi oscillations in the population between states, where the vector of state amplitudes $\boldsymbol{\mathcal{C}}^T = (\mathcal{C}_0, \mathcal{C}_x, \mathcal{C}_y, \mathcal{C}_z)$ evolves according to

$$\boldsymbol{\mathcal{C}}(t) = \exp\left[-i\begin{pmatrix} 0 & \chi_x^* & \chi_y^* & \chi_z^* \\ \chi_x & -\delta_x & 0 & 0 \\ \chi_y & 0 & -\delta_y & 0 \\ \chi_z & 0 & 0 & -\delta_z \end{pmatrix} t\right] \boldsymbol{\mathcal{C}}(0). \quad (1)$$

Here, $\chi_\mu$ is the Rabi frequency and $\delta_\mu \simeq (\omega_{1\mu} - \omega_{2\mu}) - \omega_{21}^{\mathrm{A}} - \delta_\mu^D - \delta_\mu^R$ is the two-photon detuning of each beam pair, where $\delta_\mu^D = \boldsymbol{k}_\mu \cdot \boldsymbol{v}_0$ is the Doppler shift for initial velocity $\boldsymbol{v}_0 = \boldsymbol{p}_0/m$, $\delta_\mu^R = \hbar k_\mu^2/2m$ is a photon recoil shift, and $m$ is the atomic mass. For the special case when $\delta_x = \delta_y = \delta_z \equiv \delta$, the effective Rabi frequency for this system can be written analytically as $\Omega_{\mathrm{Rabi}} = \frac{1}{2}\sqrt{\delta^2 + 4(|\chi_x|^2 + |\chi_y|^2 + |\chi_z|^2)}$.

We now discuss the specific case of 2D atom optics. Figure 2(a) displays Rabi oscillations corresponding to a 2D beam splitter, where population is transferred between atoms initially in $|1,0,0,0\rangle$ and the two diffracted states $|2,\hbar k_x,0,0\rangle$ and $|2,0,\hbar k_y,0\rangle$. A beam splitter is achieved at an interaction time $\tau$ corresponding to a pulse area $\Omega_{\mathrm{Rabi}}\tau = \pi/2$, where 50% of the population is accumulated in the two target states. Contrary to a 1D beam splitter, where one usually desires a 50/50 superposition of the initial and final states, here the population in the initial state is fully depleted—closely resembling 1D double-diffraction beam splitters [40–44]. Similarly, Fig. 2(b) shows the Rabi oscillation corresponding to a 2D mirror, where a $\pi$ pulse of duration $2\tau$ achieves 100% population transfer from $|2,0,\hbar k_y,0\rangle$ to $|2,\hbar k_x,0,0\rangle$. The resonance frequency for this transition is identical to the population-reversed case ($|2,\hbar k_x,0,0\rangle \rightarrow |2,0,\hbar k_y,0\rangle$), which is ideal for reflecting the two arms of an interferometer. We emphasize that this population transfer is possible only through the coupling with the undiffracted state $|1,0,0,0\rangle$. These 2D atom optics are similar to those proposed in Ref. [45].

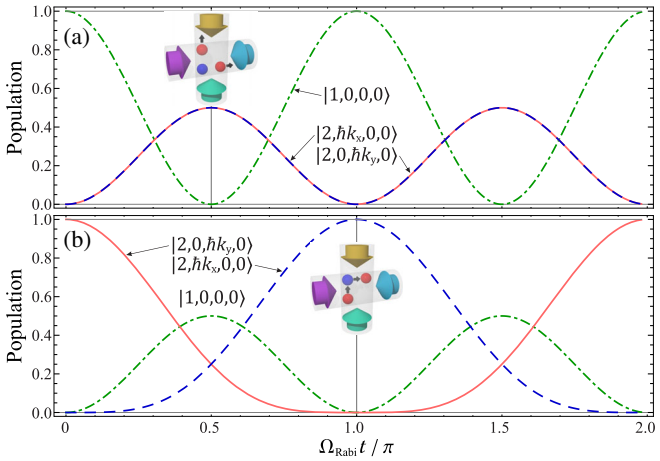


FIG. 2. Rabi oscillations for a 2D beam splitter (a) and mirror (b) realized using pulse areas of $\Omega_{\mathrm{Rabi}}t = \pi/2$ and $\pi$, respectively. The insets show the corresponding physical picture.

A key aspect of any matter-wave optical element is the transfer of a "classical" phase to the atoms [1,16,46]. In the case of light-pulse atom optics, this is the optical phase difference between excitation beams at the position of the atoms [2]. To illustrate how these optical phases play a role for 2D atom optics, we consider the specific case of resonant fields ($\delta_x = \delta_y = 0$) and Rabi frequencies of identical magnitude ($\chi_\mu = |\chi|e^{i\phi_\mu}$). Here, $\phi_\mu = \boldsymbol{k}_\mu \cdot \boldsymbol{r} + \varphi_\mu$ is the total phase difference between Raman beams along the $\mu$ axis, with the atomic position denoted by $\boldsymbol{r}$ and the laser phase difference by $\varphi_\mu = \varphi_{1\mu} - \varphi_{2\mu}$. In a truncated basis with $\boldsymbol{\mathcal{C}}^{\mathrm{T}} = (\mathcal{C}_0, \mathcal{C}_x, \mathcal{C}_y)$, the 2D beam splitter and mirror pulses can then be summarized by the following matrices:

$$\mathbb{M}_{2\mathrm{D}}(\tau) = -\begin{pmatrix} 0 & \frac{i}{\sqrt{2}}e^{-i\phi_x} & \frac{i}{\sqrt{2}}e^{-i\phi_y} \\ \frac{i}{\sqrt{2}}e^{i\phi_x} & -\frac{1}{2} & \frac{1}{2}e^{i(\phi_x-\phi_y)} \\ \frac{i}{\sqrt{2}}e^{i\phi_y} & \frac{1}{2}e^{i(\phi_y-\phi_x)} & -\frac{1}{2} \end{pmatrix}, \quad (2a)$$

$$\mathbb{M}_{2\mathrm{D}}(2\tau) = -\begin{pmatrix} 1 & 0 & 0 \\ 0 & 0 & e^{i(\phi_x-\phi_y)} \\ 0 & e^{i(\phi_y-\phi_x)} & 0 \end{pmatrix}. \quad (2b)$$

Here, the role of the optical phases becomes immediately clear. For atoms undergoing a two-photon transition from $|1,0,0,0\rangle$ to the diffracted state along axis $\mu$, the phase $\phi_\mu$ is imprinted on the wave packet. This is a result of absorbing a photon from the field propagating along $\boldsymbol{\kappa}_{1\mu}$, followed by stimulated emission into the field along $\boldsymbol{\kappa}_{2\mu}$. Similarly, the phase $-\phi_\mu$ is imprinted when making the transition from the same diffracted state back to $|1,0,0,0\rangle$. Finally, atoms transferred between diffracted states acquire the phase $\pm(\phi_x - \phi_y)$. This arises because there is no direct coupling between $|2,\hbar k_x,0,0\rangle$ and $|2,0,\hbar k_y,0\rangle$—atoms must make a four-photon transition through the intermediate state $|1,0,0,0\rangle$ in a similar manner to double diffraction [40,42].

A 2D Mach-Zehnder interferometer can be formed by combining a sequence of three 2D atom-optical pulses of duration $\tau - 2\tau - \tau$, each separated by an interrogation time $T$. Figure 3(a) shows the atomic trajectories associated with this new AI geometry, where atoms are split, reflected, and recombined along two spatial directions. A simple matrix representation of this process is obtained from the following product

$$\mathbb{M}_{\mathrm{MZ}} = \mathbb{M}_{\mathrm{2D}}(\tau)\mathbb{U}_{\mathrm{free}}(T)\mathbb{M}_{\mathrm{2D}}(2\tau)\mathbb{U}_{\mathrm{free}}(T)\mathbb{M}_{\mathrm{2D}}(\tau), \qquad (3)$$

where $\mathbb{U}_{\mathrm{free}}(T)$ is a unitary matrix describing the free evolution between laser interactions [47]. For an atom initially in $|1,0,0,0\rangle$, and allowing for different optical phases $\phi_{\mu,i}$ during the $i$th pulse, one can show that the two internal state populations—corresponding to the two complimentary output ports of the AI—are given by

$$|\langle 1|\mathbb{M}_{\mathrm{MZ}}|1,0,0,0\rangle|^2 = \frac{1}{2}(1+\cos\Delta\Phi) = |\mathcal{C}_0|^2,$$
$$|\langle 2|\mathbb{M}_{\mathrm{MZ}}|1,0,0,0\rangle|^2 = \frac{1}{2}(1-\cos\Delta\Phi) = |\mathcal{C}_x|^2 + |\mathcal{C}_y|^2,$$

where $\Delta\Phi = \Delta\phi_1 - 2\Delta\phi_2 + \Delta\phi_3$ is the total AI phase shift, with $\Delta\phi_i \equiv \phi_{x,i} - \phi_{y,i}$. We point out that the populations of the two diffracted states, $|\mathcal{C}_x|^2$ and $|\mathcal{C}_y|^2$, are identical and hence carry the same information.

The state-labeled architecture of this AI enables one to read out the two AI ports by spatial integration using resonant fluorescence or absorption imaging [48]. Although the output ports are spatially separated, the 2D AI shown in Fig. 3(a) does not require a spatially resolved detection system [49–51]. An interference fringe can be obtained from either port by scanning the optical phases—allowing one to probe for inertial effects.

The atomic trajectories shown in Fig. 3(a) give this 2D AI a unique sensitivity to inertial effects. Intuitively, since the two pathways enclose a rectangular spatial area in the $xy$ plane, the inertial phase is sensitive to the rotation component perpendicular to this plane, $\Omega_z$. This sensitivity is proportional to the area enclosed by the two pathways and does not require an initial velocity. In addition, when projected onto the $xt$ and $yt$ planes, these pathways enclose the same space-time area as a 1D Mach-Zehnder geometry—yielding sensitivity to the two acceleration components $a_x$ and $a_y$.

The full inertial dynamics resulting from the interference between any two atomic trajectories are encoded in the phase shift $\Delta\Phi$. We compute this phase shift for the 2D Mach-Zehnder geometry using the $ABCD\xi$ formalism developed by Bordé and Antoine [16,35,52,53]. Briefly, for an $N$-pulse interferometer, $\Delta\Phi$ can be written as

$$\Delta\Phi = \sum_{i=1}^{N} \Delta\boldsymbol{K}_i \cdot \boldsymbol{Q}_i + \Delta\varphi_i, \qquad (4)$$

where $\Delta\boldsymbol{K}_i \equiv \boldsymbol{k}_{A,i} - \boldsymbol{k}_{B,i}$ is the difference between the effective wave vectors $\boldsymbol{k}_{A,i}$ and $\boldsymbol{k}_{B,i}$ associated with the momentum transfer from the $i$th light pulse along paths "$A$" and "$B$," respectively. Similarly, $\boldsymbol{Q}_i \equiv \frac{1}{2}[\boldsymbol{q}_A(t_i) + \boldsymbol{q}_B(t_i)]$ is the position on the midpoint trajectory, and $\Delta\varphi_i = \varphi_{A,i} - \varphi_{B,i}$ is a control parameter arising from the relative laser phases. The atomic position and momentum trajectories, $\boldsymbol{q}(t)$ and $\boldsymbol{p}(t)$ respectfully, are computed from the solution to the classical equations of motion [52]. Because of the symmetry of the Mach-Zehnder geometry (i.e., $\boldsymbol{k}_{A,2} + \boldsymbol{k}_{B,2} = 0$), the phase shift is entirely determined by the choice of initial wave vectors $\boldsymbol{k}_{A,1}$ and $\boldsymbol{k}_{B,1}$ [54]. In what follows, we label

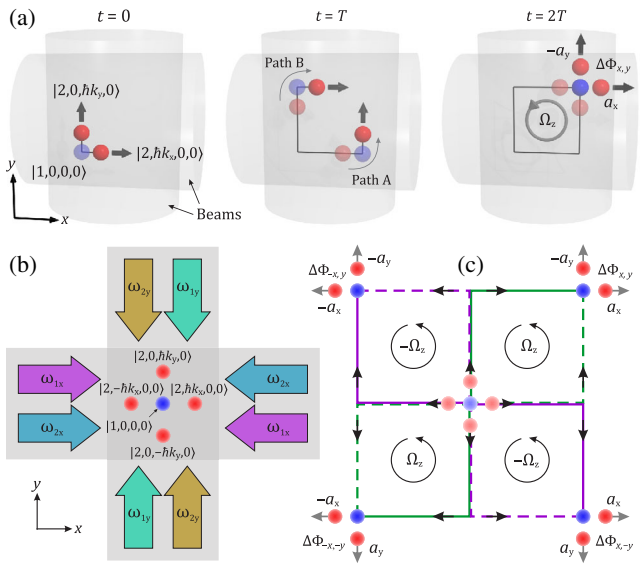


FIG. 3. (a) A sequence of 2D atom-optical pulses constituting a 2D Mach-Zehnder interferometer. (b) A retroreflected beam geometry enabling 2D double-diffraction atom optics, which symmetrically transfer $\pm\hbar k_\mu$ of momentum along each axis $\mu = x, y$. (c) Four simultaneous 2D Mach-Zehnder AIs derived from the same atomic source. Linear combinations of the four phase shifts allow one to isolate the three inertial components $a_x$, $a_y$, and $\Omega_z$ with increased sensitivity.

the AI phase shift with the subscript "$A,B$" which specifies both its geometry and initial wave vectors. To leading order in $T$, the generalized Mach-Zehnder phase shift is [36]

$$\Delta\Phi_{A,B} = \Delta\boldsymbol{K}_1 \cdot \left[\boldsymbol{a} + 2\left(\boldsymbol{v}_1 + \frac{\hbar}{m}\boldsymbol{K}_1\right) \times \boldsymbol{\Omega}\right] T^2. \quad (5)$$

Here, $\boldsymbol{a} = (a_x, a_y, a_z)$ is the acceleration vector due to external motion and gravity, $\boldsymbol{\Omega} = (\Omega_x, \Omega_y, \Omega_z)$ is the rotation vector, $\boldsymbol{v}_1$ is the atomic velocity at the time of the first light pulse, $\boldsymbol{K}_1 \equiv \frac{1}{2}(\boldsymbol{k}_{\mathrm{A},1} + \boldsymbol{k}_{\mathrm{B},1})$ corresponds to the momentum transferred to the atom's center of mass by the first pulse, and we have omitted the control phases $\Delta\varphi_i$ for clarity. The first two terms in Eq. (5) correspond to the well-known first-order phase shift $\Delta\boldsymbol{K}_1 \cdot (\boldsymbol{a} + 2\boldsymbol{v}_1 \times \boldsymbol{\Omega})T^2$, which exhibits sensitivity to the components of $\boldsymbol{a}$ and the Coriolis acceleration $2\boldsymbol{v}_1 \times \boldsymbol{\Omega}$ that are parallel to $\Delta\boldsymbol{K}_1$. The third term is a purely rotational phase which can be written as $2(\hbar/m)(\Delta\boldsymbol{K}_1 \times \boldsymbol{K}_1) \cdot \boldsymbol{\Omega}T^2$. We emphasize that this phase is not present in 1D light-pulse AIs where $\Delta\boldsymbol{K}_1 \times \boldsymbol{K}_1 = 0$. This key point leads to additional rotation and gravity gradient sensitivity [36] with multidimensional geometries that has not yet been exploited experimentally. In contrast to previous atomic gyroscopes [26–32], here an initial launch velocity is not required to achieve rotation sensitivity—instead this velocity is provided by the first 2D beam splitter. This is advantageous for two reasons: (i) the magnitude of this velocity kick can be as precise as the value of $k$ (typically better than one part in $10^9$), and (ii) the direction of the kick can be changed by simply reversing the sign of $\boldsymbol{k}_{A,1}$ and $\boldsymbol{k}_{B,1}$. With a single atomic source, these features can then be exploited to suppress contributions from pure accelerations and initial velocities—which are the main sources of error in atomic gyroscopes [28].

For the 2D Mach-Zehnder geometry shown in Fig. 3(a), with initial wave vectors in the $xy$ plane ($\boldsymbol{k}_{A,1} = k_x\hat{\boldsymbol{x}}$, $\boldsymbol{k}_{B,1} = k_y\hat{\boldsymbol{y}}$, $\Delta\boldsymbol{K}_1 \times \boldsymbol{K}_1 = k_x k_y \hat{\boldsymbol{z}}$), Eq. (5) gives

$$\Delta\Phi_{x,y} = k_x a_x^{\mathrm{tot}} T^2 - k_y a_y^{\mathrm{tot}} T^2 + \frac{2\hbar}{m} k_x k_y \Omega_z T^2, \quad (6)$$

where $\boldsymbol{a}^{\mathrm{tot}} \equiv \boldsymbol{a} + 2\boldsymbol{v}_1 \times \boldsymbol{\Omega}$. Although this phase contains a mixture of different inertial effects, one can isolate each of them by using linear combinations of phases obtained from area-reversed geometries, as shown in Table I. Each phase $\Delta\Phi_{A,B}$ can be obtained from a single measurement by employing double-diffraction [40–44] or double-single-diffraction [55] atom optics in two dimensions [36]. Figures 3(b) and 3(c) display a scheme in which four simultaneous interferometers are generated from the same atomic source via 2D double diffraction pulses—enabling one to isolate $a_x$, $a_y$, and $\Omega_z$ in a single shot. Here, the phase readout requires spatial resolution of the adjacent interferometer ports; therefore the cloud diameter at the final beam splitter must be less than the separation between adjacent clouds. This implies a sub-recoil-cooled source with an initial cloud size $\sigma_0 \ll 2\hbar k_\mu T/m$ (e.g., $\sigma_0 \ll 1$ mm for $T = 10$ ms). This scheme is well suited to inertial navigation applications, where strong variations of rotations and accelerations between measurement cycles would compromise the common-mode rejection of a sequential measurement protocol. Additionally, with strongly correlated measurements, one can reject both the phase noise between orthogonal Raman beams and common systematic effects.

TABLE I. Linear combinations of 2D Mach-Zehnder phases obtained from the four symmetric geometries shown in Fig. 3(c). Here, the laser phase contribution $\Delta\varphi_1 - 2\Delta\varphi_2 + \Delta\varphi_3$ cancels in the sum phase since it is common to all geometries.

| $\Delta\Phi_{x,y}$ | $\Delta\Phi_{-x,y}$ | $\Delta\Phi_{-x,-y}$ | $\Delta\Phi_{x,-y}$ | Sum phase |
|---|---|---|---|---|
| + | − | − | + | $4k_x a_x^{\mathrm{tot}} T^2$ |
| − | − | + | + | $4k_y a_y^{\mathrm{tot}} T^2$ |
| + | − | + | − | $8(\hbar/m)k_x k_y \Omega_z T^2$ |

These principles can be extended to a 3D geometry, where three mutually perpendicular pairs of Raman beams intersect to generate three separate 2D interferometers in orthogonal planes, as shown in Fig. 4. At $t = 0$, a 3D beam splitter diffracts an atom initially in the undiffracted state $|1,0,0,0\rangle$ into three equal proportions traveling along $\hat{\boldsymbol{x}}$, $\hat{\boldsymbol{y}}$, and $\hat{\boldsymbol{z}}$. These three diffracted states continue along their respective axes ($\hat{\boldsymbol{\mu}}$) until $t = T$, when a 3D atom-optical mirror freezes the motion along $\hat{\boldsymbol{\mu}}$ and diffracts each wave packet equally along the two directions orthogonal to $\hat{\boldsymbol{\mu}}$ [56]. Finally, at $t = 2T$ the atoms intersect at three opposite corners of a cube, as shown in Fig. 4(c), where a recombination pulse transfers population from the diffracted states in each plane to an undiffracted one. Detection of the resulting 9 spatially separated clouds yields sensitivity to the full acceleration and rotation vectors in a single shot. Individual inertial components can then be isolated in the same manner previously

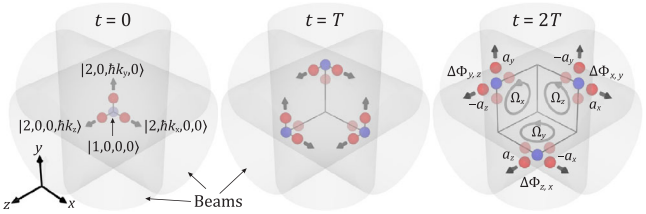


FIG. 4. A sequence of 3D atom optical pulses generating three 2D Mach-Zehnder interferometers in mutually orthogonal planes. Parasitic trajectories excited by the beams are not shown. Three sets of spatially separated atomic clouds arrive at opposite corners of a cube where they can be read out simultaneously—yielding sensitivity to the full acceleration and rotation vectors.

described for a 2D geometry—that is, by exciting symmetrically with double-diffraction pulses and imaging the clouds separately in each plane.

This 3D geometry allows one to easily construct a three-axis gyroscope. For instance, the combination of phases: $\Theta \equiv \Delta\Phi_{x,y} + \Delta\Phi_{y,z} + \Delta\Phi_{z,x}$, obtained from three corners of the cube, and $\Upsilon \equiv \Delta\Phi_{-x,y} + \Delta\Phi_{y,z} + \Delta\Phi_{z,-x}$, acquired by reversing the Raman wave vector on the $x$ axis, yields

$$\Theta = \frac{2\hbar}{m}(k_y k_z \Omega_x + k_x k_z \Omega_y + k_x k_y \Omega_z) T^2, \tag{7a}$$

$$\Upsilon = \frac{2\hbar}{m}(k_y k_z \Omega_x - k_x k_z \Omega_y - k_x k_y \Omega_z) T^2. \tag{7b}$$

These phase combinations allow one to access $\Omega_x$ through the sum $\Theta + \Upsilon = 4\frac{\hbar}{m} k_y k_z \Omega_x T^2$. Hence, Eq. (7) can be used as a building block to isolate each rotation component. A key point here is that both $\Theta$ and $\Upsilon$ arise from a single measurement of three simultaneous 2D interferometers in orthogonal planes. Yet they are each immune to spurious velocities, accelerations, and laser phase noise, and hence can be combined to isolate a given rotation component. Since all quantities appearing in these rotation phases are precisely known, future gyroscopes based on this architecture could benefit from the same relative accuracy as cold-atom-based accelerometers [5].

We have presented a novel approach for manipulating atomic wave packets in multiple spatial dimensions. These new atom-optical tools can be utilized to generate simple 2D interferometers sensitive to inertial effects in three dimensions. More complex planar geometries involving 2D double diffraction pulses enable one to isolate two components of acceleration and one rotation in a single shot, while also rejecting laser phase noise and common systematic effects. Finally, we discussed an extension to a 3D geometry, where the full acceleration and rotation vectors can be retrieved. These concepts can easily be extended to other AI configurations involving four or more pulses [57,58], which could be advantageous for applications such as multi-axis gravity gradiometry, gyroscopy, or gravitational wave detection. The sensitivity of these AIs could also benefit from multiphoton momentum transfer pulses [59–64], which would aid the realization of a 3D inertial sensor in a compact volume. We anticipate that this work will influence future generations of quantum accelerometers and gyroscopes, and will offer new perspectives for inertial navigation systems.

This work is supported by the French national agencies ANR (Agence Nationale de la Recherche), and DGA (Direction Générale de l'Armement) under Grant No. ANR-17-ASTR-0025-01. P. B. thanks Conseil Régional d'Aquitaine for the Excellence Chair.

*Corresponding author.
brynle.barrett@ixblue.com

[1] Ch. J. Bordé, Atom interferometry with internal state labelling, Phys. Lett. A **140**, 10 (1989).
[2] M. A. Kasevich and S. Chu, Atomic Interferometry Using Stimulated Raman Transitions, Phys. Rev. Lett. **67**, 181 (1991).
[3] A. Cronin, J. Schmiedmayer, and D. E. Pritchard, Optics and interferometry with atoms and molecules, Rev. Mod. Phys. **81**, 1051 (2009).
[4] O. Carraz, C. Siemes, L. Massotti, R. Haagmans, and P. Silvestrin, A spaceborne gravity gradiometer concept based on cold atom interferometers for measuring earth's gravity field, Microgravity Sci. Technol. **26**, 139 (2014).
[5] V. Ménoret, P. Vermeulen, N. Le Moigne, S. Bonvalot, P. Bouyer, A. Landragin, and B. Desruelle, Gravity measurements below $10^{-9}$ g with a transportable absolute quantum gravimeter, Sci. Rep. **8**, 12300 (2018).
[6] B. Canuel *et al.*, Exploring gravity with the MIGA large scale atom interferometer, Sci. Rep. **8**, 14064 (2018).
[7] J. M. Hogan, D. M. S. Johnson, and M. A. Kasevich, in *Proceedings of the International School of Physics "Enrico Fermi"*, edited by E. Arimondo, W. Ertmer, W. P. Schleich, and E. M. Rasel (IOS, Amsterdam; SIF, Bologna, 2009), Vol. 168, pp. 411–447.
[8] B. Barrett, P.-A. Gominet, E. Cantin, L. Antoni-Micollier, A. Bertoldi, B. Battelier, P. Bouyer, J. Lautier, and A. Landragin, in *Proceedings of the International School of Physics "Enrico Fermi"*, edited by G. M. Tino and M. A. Kasevich (IOS, Amsterdam; SIF, Bologna, 2014), Vol. 188, pp. 493–555.
[9] R. Bouchendira, P. Cladé, S. Guellati-Khélifa, F. Nez, and F. Biraben, New Determination of the Fine Structure Constant and Test of the Quantum Electrodynamics, Phys. Rev. Lett. **106**, 080801 (2011).
[10] G. Rosi, F. Sorrentino, L. Cacciapuoti, M. Prevedelli, and G. M. Tino, Precision measurement of the Newtonian gravitational constant using cold atoms, Nature (London) **510**, 518 (2014).
[11] D. Becker *et al.*, Space-borne Bose-Einstein condensation for precision interferometry, Nature (London) **562**, 391 (2018).
[12] C. Jekeli, Navigation error analysis of atom interferometer inertial sensor, Navigation **52**, 1 (2005).
[13] B. Battelier, B. Barrett, L. Fouché, L. Chichet, L. Antoni-Micollier, H. Porte, F. Napolitano, J. Lautier, A. Landragin, and P. Bouyer, Development of compact cold-atom sensors for inertial navigation, in *Proceedings of SPIE Quantum Optics* (SPIE Press, Cardiff, 2016), Vol. 9900, p. 990004.
[14] B. Fang, I. Dutta, P. Gillot, D. Savoie, J. Lautier, B. Cheng, C. L. Garrido Alzar, R. Geiger, S. Merlet, F. Pereira Dos Santos, and A. Landragin, Metrology with atom interferometry: Inertial sensors from laboratory to field applications, J. Phys.: Conf. Ser. **723**, 012049 (2016).
[15] P. Cheiney, L. Fouché, S. Templier, F. Napolitano, B. Battelier, P. Bouyer, and B. Barrett, Navigation-Compatible Hybrid Quantum Accelerometer using a Kalman Filter, Phys. Rev. Applied **10**, 034030 (2018).
[16] Ch. J. Bordé, Theoretical tools for atom optics, and interferometry, C. R. Acad. Sci. (Paris) **2**, 509 (2001).

[17] T. M. Niebauer, G. S. Sasagawa, J. E. Faller, R. Hilt, and F. Klopping, A new generation of absolute gravimeters, Metrologia **32**, 159 (1995).
[18] A. Peters, K. Y. Chung, and S. Chu, Measurement of gravitational acceleration by dropping atoms, Nature (London) **400**, 849 (1999).
[19] P. Gillot, O. Francis, A. Landragin, F. Pereira Dos Santos, and S. Merlet, Stability comparison of two absolute gravimeters: Optical versus atomic interferometers, Metrologia **51**, L15 (2014).
[20] C. Freier, M. Hauth, V. Schkolnik, B. Leykauf, M. Schilling, H. Wziontek, H.-G. Scherneck, J. Muller, and A. Peters, Mobile quantum gravity sensor with unprecedented stability, J. Phys.: Conf. Ser. **723**, 012050 (2016).
[21] K. S. Hardman, P. J. Everitt, G. D. McDonald, P. Manju, P. B. Wigley, M. A. Sooriyabandara, C. C. N. Kuhn, J. E. Debs, J. D. Close, and N. P. Robins, Simultaneous Precision Gravimetry and Magnetic Gradiometry with a Bose-Einstein Condensate: A High Precision, Quantum Sensor, Phys. Rev. Lett. **117**, 138501 (2016).
[22] Y. Bidel, N. Zahzam, C. Blanchard, A. Bonnin, M. Cadoret, A. Bresson, D. Rouxel, and M. F. Lequentrec-Lalancette, Absolute marine gravimetry with matter-wave interferometry, Nat. Commun. **9**, 627 (2018).
[23] M. J. Snadden, J. M. McGuirk, P. Bouyer, K. G. Haritos, and M. A. Kasevich, Measurement of the Earth's Gravity Gradient with an Atom Interferometer-Based Gravity Gradiometer, Phys. Rev. Lett. **81**, 971 (1998).
[24] G. Rosi, L. Cacciapuoti, F. Sorrentino, M. Menchetti, M. Prevedelli, and G. M. Tino, Measurement of the Gravity-Field Curvature by Atom Interferometry, Phys. Rev. Lett. **114**, 013001 (2015).
[25] P. Asenbaum, C. Overstreet, T. Kovachy, D. D. Brown, J. M. Hogan, and M. A. Kasevich, Phase Shift in an Atom Interferometer due to Spacetime Curvature across its Wave Function, Phys. Rev. Lett. **118**, 183602 (2017).
[26] T. L. Gustavson, P. Bouyer, and M. A. Kasevich, Precision Rotation Measurements with an Atom Interferometer Gyroscope, Phys. Rev. Lett. **78**, 2046 (1997).
[27] J. K. Stockton, K. Takase, and M. A. Kasevich, Absolute Geodetic Rotation Measurement Using Atom Interferometry, Phys. Rev. Lett. **107**, 133001 (2011).
[28] B. Barrett, R. Geiger, I. Dutta, M. Meunier, B. Canuel, A. Gauguet, P. Bouyer, and A. Landragin, The Sagnac effect: 20 years of development in matter-wave interferometry, C.R. Phys. **15**, 875 (2014).
[29] G. Tackmann, P. Berg, S. Abend, C. Schubert, W. Ertmer, and E. M. Rasel, Large-area Sagnac atom interferometer with robust phase read out, C.R. Phys. **15**, 884 (2014).
[30] A. V. Rakholia, H. J. McGuinness, and G. W. Biedermann, Dual-Axis High-Data-Rate Atom Interferometer via Cold Ensemble Exchange, Phys. Rev. Applied **2**, 054012 (2014).
[31] I. Dutta, D. Savoie, B. Fang, B. Venon, C. L. Garrido Alzar, R. Geiger, and A. Landragin, Continuous Cold-Atom Inertial Sensor with 1 nrad/sec Rotation Stability, Phys. Rev. Lett. **116**, 183003 (2016).
[32] Z. W. Yao, S. B. Lu, R. B. Li, J. Luo, J. Wang, and M. S. Zhan, Calibration of atomic trajectories in a large-area dual-atom-interferometer gyroscope, Phys. Rev. A **97**, 013620 (2018).
[33] B. Canuel, F. Leduc, D. Holleville, A. Gauguet, J. Fils, A. Virdis, A. Clairon, N. Dimarcq, Ch. J. Bordé, A. Landragin, and P. Bouyer, Six-Axis Inertial Sensor Using Cold-Atom Interferometry, Phys. Rev. Lett. **97**, 010402 (2006).
[34] X. Wu, F. Zi, J. Dudley, R. J. Bilotta, P. Canoza, and H. Müller, Multiaxis atom interferometry with a single-diode laser and a pyramidal magneto-optical trap, Optica **4**, 1545 (2017).
[35] Ch. J. Bordé, Quantum theory of atom-wave beam splitters and application to multidimensional atomic gravito-inertial sensors, Gen. Relativ. Gravit. **36**, 475 (2004).
[36] See Supplemental Material at http://link.aps.org/supplemental/10.1103/PhysRevLett.122.043604 for a more detailed analysis of multidimensional atom optics and interferometer phase shifts.
[37] These multidimensional atom optics can also be achieved using Bragg transitions.
[38] A. Aspect, E. Arimondo, R. Kaiser, N. Vansteenkiste, and C. Cohen-Tannoudji, Laser cooling below the one-photon recoil energy by velocity-selective coherent population trapping: Theoretical analysis, J. Opt. Soc. Am. B **6**, 2112 (1989).
[39] K. Moler, D. S. Weiss, M. Kasevich, and S. Chu, Theoretical analysis of velocity-selective Raman transitions, Phys. Rev. A **45**, 342 (1992).
[40] T. Lévèque, A. Gauguet, F. Michaud, F. Pereira Dos Santos, and A. Landragin, Enhancing the Area of a Raman Atom Interferometer Using a Versatile Double-Diffraction Technique, Phys. Rev. Lett. **103**, 080405 (2009).
[41] N. Malossi, Q. Bodart, S. Merlet, T. Lévèque, A. Landragin, and F. Pereira Dos Santos, Double diffraction in an atomic gravimeter, Phys. Rev. A **81**, 013617 (2010).
[42] E. Giese, A. Roura, G. Tackmann, E. M. Rasel, and W. P. Schleich, Double Bragg diffraction: A tool for atom optics, Phys. Rev. A **88**, 053608 (2013).
[43] J. Küber, F. Schmaltz, and G. Birkl, Experimental realization of double Bragg diffraction: Robust beamsplitters, mirrors, and interferometers for Bose-Einstein condensates, arXiv:1603.08826.
[44] H. Ahlers, H. Müntinga, A. Wenzlawski, M. Krutzik, G. Tackmann, S. Abend, N. Gaaloul, E. Giese, A. Roura, R. Kuhl, C. Lämmerzahl, A. Peters, P. Windpassinger, K. Sengstock, W. P. Schleich, W. Ertmer, and E. M. Rasel, Double Bragg Interferometry, Phys. Rev. Lett. **116**, 173601 (2016).
[45] R. Geiger and M. Trupke, Proposal for a Quantum Test of the Weak Equivalence Principle with Entangled Atomic Species, Phys. Rev. Lett. **120**, 043602 (2018).
[46] C. Cohen-Tannoudji, J. Dupont-Roc, and G. Grynberg, *Atom-Photon Interactions: Basic Process and Applications* (John Wiley & Sons, Inc., New York, 1992).
[47] P. Cheinet, B. Canuel, F. Pereira Dos Santos, A. Gauguet, F. Yver-Leduc, and A. Landragin, Measurement of the sensitivity function in a time-domain atomic interferometer, IEEE Trans. Instrum. Meas. **57**, 1141 (2008).
[48] E. Rocco, R. N. Palmer, T. Valenzuela, V. Boyer, A. Freise, and K. Bongs, Fluorescence detection at the atom shot noise limit for atom interferometry, New J. Phys. **16**, 093046 (2014).

[49] S. M. Dickerson, J. M. Hogan, A. Sugarbaker, D. M. S. Johnson, and M. A. Kasevich, Multiaxis Inertial Sensing with Long-Time Point Source Atom Interferometry, Phys. Rev. Lett. **111**, 083001 (2013).

[50] A. Sugarbaker, S. M. Dickerson, J. M. Hogan, D. M. S. Johnson, and M. A. Kasevich, Enhanced Atom Interferometer Readout Through the Application of Phase Shear, Phys. Rev. Lett. **111**, 113002 (2013).

[51] G. W. Hoth, B. Pelle, S. Riedl, J. Kitching, and E. A. Donley, Point source atom interferometry with a cloud of finite size, Appl. Phys. Lett. **109**, 071113 (2016).

[52] Ch. Antoine and Ch. J. Bordé, Exact phase shifts for atom interferometry, Phys. Lett. A **306**, 277 (2003).

[53] Ch. Antoine and Ch. J. Bordé, Quantum theory of atomic clocks and gravito-inertial sensors: An update, J. Opt. B **5**, S199 (2003).

[54] The final wave vectors are predetermined by the initial wave vectors in order to close the two interferometer arms, i.e., $\boldsymbol{k}_{\mathrm{A},1} + \boldsymbol{k}_{\mathrm{B},3} = 0$ and $\boldsymbol{k}_{\mathrm{A},3} + \boldsymbol{k}_{\mathrm{B},1} = 0$.

[55] B. Barrett, L. Antoni-Micollier, L. Chichet, B. Battelier, T. Lévèque, A. Landragin, and P. Bouyer, Dual matter-wave inertial sensors in weightlessness, Nat. Commun. **7**, 13786 (2016).

[56] After the 3D mirror pulse, $1/9$ of the population on each arm remains in the undiffracted state (not shown in Fig. 4), which leads to a loss of interference contrast.

[57] B. Dubetsky and M. A. Kasevich, Atom interferometer as a selective sensor of rotation or gravity, Phys. Rev. A **74**, 023615 (2006).

[58] M. Cadoret, N. Zahzam, Y. Bidel, C. Diboune, A. Bonnin, F. Théron, and A. Bresson, A phase shift formulation for N-light-pulse atom interferometers: Application to inertial sensing, J. Opt. Soc. Am. B **33**, 1777 (2016).

[59] V. S. Malinovsky and P. R. Berman, Momentum transfer using chirped standing wave fields: Bragg scattering, Phys. Rev. A **68**, 023610 (2003).

[60] P. Cladé, S. Guellati-Khélifa, F. Nez, and F. Biraben, Large Momentum Beam Splitter Using Bloch Oscillations, Phys. Rev. Lett. **102**, 240402 (2009).

[61] T. Kovachy, S.-w. Chiow, and M. A. Kasevich, Adiabatic-rapid-passage multiphoton Bragg atom optics, Phys. Rev. A **86**, 011606 (2012).

[62] G. D. McDonald, C. C. N. Kuhn, S. Bennetts, J. E. Debs, K. S. Hardman, M. Johnsson, J. D. Close, and N. P. Robins, 80hk momentum separation with Bloch oscillations in an optically guided atom interferometer, Phys. Rev. A **88**, 053620 (2013).

[63] K. Kotru, D. L. Butts, J. M. Kinast, and R. E. Stoner, Large-Area Atom Interferometry with Frequency-Swept Raman Adiabatic Passage, Phys. Rev. Lett. **115**, 103001 (2015).

[64] M. Jaffe, V. Xu, P. Haslinger, H. Müller, and P. Hamilton, Efficient Adiabatic Spin-Dependent Kicks in an Atom Interferometer, Phys. Rev. Lett. **121**, 040402 (2018).